Theoretical investigation of the ^{67}Zn Mössbauer isomer shifts in the zinc chalcogenides

A. Svane* and E. Antoncik
Institute of Physics, University of Aarhus, DK-8000 Aarhus C, Denmark
(Received 3 December 1985)

The band structures of the zinc chalcogenides ZnO, ZnS, ZnSe, and ZnTe having the sphalerite crystal structure are calculated. The first-principles linear muffin-tin-orbital—atomic sphere approximation method is employed, in which all solid-state and scalar relativistic effects are taken into account, including the self-consistency of the crystal potential and the charge density. The corresponding electronic configurations are discussed, and the electron contact densities at the zinc nucleus are obtained and compared to experimental isomer-shift data with good agreement. The estimated static charge transfers of the zinc chalcogenides are demonstrated to correlate neatly with the isomer shift. For the first time an accurate value of the calibration constant for the ^{67}Zn isomer transition is derived: $\Delta R/R=(7.0\pm1.0)\times10^{-4}$.

I. INTRODUCTION

The Mössbauer isomer shift[1] provides a unique experimental technique for studying the electronic structure of solids on an atomic scale. With this technique the solid-state physicist may investigate the local chemical bond in pure crystalline materials as well as more complicated systems like impurities in solids and amorphous and implanted materials. For basic research on elemental semiconductors and semiconducting compounds the ^{119}Sn Mössbauer isotope has proven valuable as a probe to monitor the local electronic configuration. Thus, when substitutionally implanted in the group-IV semiconductors,[2] and III-V compounds,[3] the measured isomer shift provides information on the electronic and vibronic properties of the host crystal.[4–7] Similar investigations have been performed with the ^{125}Te and ^{129}I isotopes,[8,9] and more recently with the ^{121}Sb isotope,[10] but many other Mössbauer isotopes are likely to become useful in this respect.

The ^{67}Zn isotope is one such candidate holding the promise of becoming a prominent spectroscopic tool in the study of semiconductor physics. This is primarily due to the extreme narrow width of the isomeric transition of ^{67}Zn, with a natural linewidth $\Gamma_0\sim50$ peV, so that a probe of very high resolution is at hand. Furthermore, Zn, as a divalent atom, in a chemical sense is complementary to the more conventional Mössbauer isotopes of Sn, Sb, Te, and I. The experimental conditions for performing ^{67}Zn Mössbauer spectroscopy are, however, more complicated than for the other isotopes mentioned. This is due to the low resonance effect and to the requirement of a very sensitive velocity spectrometer to resolve the resonance line. Also, experiments must be performed at liquid-He temperature to minimize the effects of the second-order Doppler shift. For a general review of the history and achievements of ^{67}Zn Mössbauer spectroscopy, see Ref. 11. The proper use of the ^{67}Zn isotope as a spectroscopic tool necessitates, however, a reliable calibration of the transition, which is the aim of the present work.

The isomer shift is related to the change in transition energy between two nuclear levels, which is caused by the electrostatic interaction of the nuclear charge distributions with the surrounding electron gas. Specifically,[12]

$$\Delta_{\rm IS}=\alpha(\rho_a(0)-\rho_s(0)) , \tag{1}$$

where $\Delta_{\rm IS}$ is the resonant isomer shift velocity, $\rho_a(0)$ and $\rho_s(0)$ are the electron densities at the nuclei (the contact densities) in the absorber and source materials, respectively, and α is the so-called calibration constant[13]

$$\alpha=\beta\Delta\langle r^2\rangle . \tag{2}$$

Here β is a numerical constant,[13] $\langle r^2\rangle$ is the mean-square radius of the nuclear charge distribution, and $\Delta\langle r^2\rangle$ is the difference of this quantity between the two states. The nuclear charge distribution is usually assumed to be spherical and homogeneous, in which case $\Delta\langle r^2\rangle$ can be written to the first order in the relative difference in radius, $\Delta R/R$, as follows:

$$\Delta\langle r^2\rangle=\tfrac{6}{5}R^2\frac{\Delta R}{R} . \tag{3}$$

This is, of course, a much too crude model for the complicated nuclear states, and Eq. (3) should not be taken as more than a parametrization of the more correct expression (2) in terms of the physically appealing quantity $\Delta R/R$.

The calibration constant α, Eq. (2), is important in connection with the extraction of useful information from isomer-shift measurements, as it enables the conversion to density units. Basically, it ought to be determinable from purely nuclear-physics models, but these have not yet reached a level of accuracy that suffices for the present purpose, though attempts have been made.[14] The most common calibration procedure of isomer resonances therefore relies on calculated electron contact densities, which are compared to experimental isomer shifts. Generally, the use of atomic calculation has been widespread, though recently molecular and cluster calculations have also been reported for some isotopes. To use atomic calculations

for the calibration of isomer shifts one needs as extra input the assumption or estimate of some atomic configuration, which can be taken as equivalent to the actual configuration of the solid. The crudeness of this and similar approximations has been well recognized,[15] but until recently very little has been attempted to improve the calibrations. In this work we take the point of view that the calibration of Mössbauer isomer shifts, being by definition a solid-state effect, should be performed using a rigorous solid-state scheme for calculating the electronic structure.

Several attempts have already been tried to account for the influence of the solid state on the electronic structure of the Mössbauer atom. Thus, the Wigner-Seitz model[16] confines the atom to a finite sphere, which represents the amount of space allotted to the atom in the solid. This widely used approximation introduces as an extra parameter the radius of the sphere, and the proper value of this is not always easy to assess.[15] Perhaps, the best attempts to calibrate Mössbauer isotopes along these lines are those calculations which derive the equivalent atomic configuration—in terms of the effective (fractional) occupancy numbers Z_s and Z_p—from parametrized tight-binding calculations.[15,17] Subsequently, the electron contact density of the (spatially confined) atom in the configuration $ns^{Z_s}np^{Z_p}$ is calculated from a Dirac-Fock-Slater procedure. In this approach no presumptions on the electronic configuration of the Mössbauer atom is needed, but rather, this information is derived from a solid-state scheme. However, a number of adjustable parameters are still present in such calculations, and they should only be regarded as a first step towards the proper incorporation of solid-state effects into the calibration procedure.

The chemical shifts of the zinc chalcogenides ZnO, ZnS, ZnSe, and ZnTe have been measured by two groups,[18,19] and the calibration of the ^{67}Zn isotope of the present work is performed by calculating the electron contact densities of these materials, which are then compared to experiments. The crystal structure of ZnS, ZnSe, and ZnTe is sphalerite (zinc blende), whereas ZnO is found in a (slightly distorted) wurtzite structure. For simplicity we have assumed that ZnO also possesses a sphalerite structure, at the same density as natural ZnO. This approximation should not be too serious for the purpose of calculating the electron contact density, as the sphalerite and wurtzite structures are quite similar, differing only in the number of third-nearest neighbors. In all cases the atomic cores were treated as frozen, thus only contributing a constant to the electron contact density. This approximation turns out to be reasonable for the zinc chalcogenides, as will be demonstrated in Sec. IV.

The linear muffin-tin-orbital (LMTO) method[20,21] is adopted for this project, as this method has proven fast and reliable for determining the electronic structure of a variety of solid-state systems such as metals, semiconductors, and surfaces. In contrast to the tight-binding method mentioned above, this scheme allows the crystal potential and charge distribution to be iterated to self-consistency. The LMTO method usually employs the atomic sphere approximation (ASA), according to which the crystal unit cell is approximated by spheres around the atomic sites. ASA is not a necessity in the LMTO formalism but represents a major simplification of the calculations with only minor drawbacks. In the ASA the crystal wave function is therefore naturally decomposed according to its angular momentum character, and the numbers of electrons having the s, p, and d character within each sphere are very convenient parameters describing the electronic structure of the solid under study. These occupancy numbers are the reminiscence of the atomic effective occupancies, Z_s and Z_p mentioned above, but in the LMTO method they are always intimately connected to a sphere of given radius.

In Sec. II we present and discuss the basic features of the LMTO-ASA method. The calculations of the zinc chalcogenides are presented in Sec. III, where the energy-band structures are exposed and compared to experiments, and the trends in the electronic structure are discussed in terms of the occupancy numbers. In Sec. IV the calibration of the ^{67}Zn resonance is performed, and the frozen-core approximation is investigated. Finally, Sec. V summarizes and concludes the achievements of the present work.

II. THE LMTO METHOD

Although the LMTO method is by now well established in solid-state physics, so far little attention has been paid to it by Mössbauer spectroscopists; therefore, a very concise review of the method will be reproduced here to facilitate the discussion of the results obtained in the following section. The method is thoroughly discussed in Refs. 20 and 21.

The Hamiltonian for a system of interacting electrons in a solid can be greatly simplified by the theorems of density-functional theory,[22–24] according to which all ground-state properties can be derived from the solutions of the one-particle Hamiltonian:

$$H(\mathbf{r}) = -\nabla^2 + V_{\text{ext}}(\mathbf{r}) + V_H(\mathbf{r}) + V_{\text{xc}}(\mathbf{r}) \ . \tag{4}$$

Here the potential is decomposed into the external, V_{ext}, the Hartree, V_H, and the exchange-correlation, V_{xc}, parts; throughout this work we use the local-density approximation with the parametrization of V_{xc} as provided by Vosko, Wilk, and Nusair.[25]

In the LMTO method the wave functions for a given $\mathbf{k}$ point in the Brillouin zone are sought as a linear combination of Bloch sums of muffin-tin orbitals,

$$\psi^{\mathbf{k}}(\mathbf{r}) = \sum_L a_L^{\mathbf{k}} \sum_{\mathbf{R}} e^{i\mathbf{k}\cdot\mathbf{R}} \chi_L(\mathbf{r}-\mathbf{R}) \ . \tag{5}$$

Here $\mathbf{R}$ denotes the lattice points and L is a combined index, $L=(\mathbf{q},l,m)$, where $\mathbf{q}$ labels the atoms within the basis and l,m are the usual angular momentum quantum numbers.

To determine the muffin-tin orbitals χ_L, true crystalline potential is replaced by a potential which is spherically symmetric inside touching spheres centered on the atomic positions and constant in the remaining parts of space. Inside the muffin-tin sphere the basic function is expanded in spherical harmonics times a radial function ψ_L and its energy derivative $\dot{\psi}_l$:

$$\psi_l(r,E) = \psi_l(r,E_{\nu l}) + (E-E_{\nu l})\dot{\psi}_l(r,E_{\nu l}) \ . \tag{6}$$

The radial function ψ_l is obtained by solving the Dirac equation in the limit of zero spin-orbit coupling at an appropriately chosen energy E_{vl}.[21] Expansion (6) has proved accurate over ranges of order 1 Ry corresponding to typical valence bandwidths in solids. The radial function has to be matched to the solutions outside the atomic spheres so that the resulting muffin-tin orbital χ_L is everywhere continuous and differentiable.

The muffin-tin approximation appears to be rather poor for open structures like the diamond and sphalerite structures, as $\sim\frac{2}{3}$ of the crystal volume is exterior to the muffin-tin spheres in the region where the potential is assigned a constant value. It was therefore suggested by Keller[26] to introduce additional "empty" spheres on high symmetry interstitial sites and allow for a radial degree of freedom of the potential within these. Accordingly, in the sphalerite structure **R**'s form the fcc lattice and the basis consists of four points, which we take to be the cation site at $\mathbf{q}_1=(0,0,0)$, the anion site at $\mathbf{q}_2=\frac{1}{4}a(1,1,1)$, and the two sites of the centers of the empty spheres, E_1 at $\mathbf{q}_3=\frac{1}{2}a(1,1,1)$ and E_2 at $\mathbf{q}_4=\frac{3}{4}a(1,1,1)$.

The energy eigenvalues $E^{\mathbf{k}}$ and the coefficients $a_L^{\mathbf{k}}$ are obtained by numerical diagonalization of the secular equation

$$\sum_L (H_{L'L}^{\mathbf{k}}-E^{\mathbf{k}}O_{L'L}^{\mathbf{k}})a_L^{\mathbf{k}}=0\ . \tag{7}$$

Both the matrix elements of the Hamiltonian $H_{L'L}$ and the overlap matrix $O_{L'L}$ are rather lengthy and can be found in Ref. 21. The knowledge of $a_L^{\mathbf{k}}$ makes it possible to calculate the wave functions (5) and, consequently, the crystal charge distribution. This may be used to construct a new potential in the Hamiltonian (4), or if self-consistency has been achieved, the contact density may be determined. It is important to stress, however, that the density-functional theory from the onset is incapable of revealing anything about excited states, and also that the mere interpretation of the eigenvalues $E^{\mathbf{k}}$ of (7) as one-particle energies is not formally justified. This is often disregarded, and indeed, in Sec. III we will compare our calculated eigenvalues for the zinc chalcogenides with experimentally derived electron energies. On the other hand, the total ground-state energy may be calculated, e.g., for the study of equilibrium parameters, pressure-dependent structural phase transformations,[27,28] or phonon spectra.[29]

Usually, in applications of the LMTO method to solids, the muffin-tin approximation is furthermore replaced by the atomic sphere approximation (ASA), in which the touching muffin-tin spheres are expanded a little to include all of space. The ASA improves on the muffin-tin approximation by allowing for a spatial variation of the potential in the whole unit cell, but the price to be paid is a violation of geometry. The conceptual and computational simplifications of the ASA are, however, significant. With these two improvements on the muffin-tin approximation the band structure, equilibrium lattice constants, and bulk moduli of the group-IV elements C, Si, and Ge (Ref. 30) and the III-V compound GaAs (Refs. 31 and 32) have been calculated with good accuracy.

In the present work the first-order correction term for the overlap of spheres derived by Andersen was also included, as was the leading nonspherical component of the potential.[33,34] The basis of muffin-tin orbitals included s, p, and d orbitals, whereby the size of the secular matrix (7) becomes 36×36. The summation over **k** points in the Brillouin zone was performed by the tetrahedron method,[35,21] using a grid of 89 **k** points within the irreducible wedge ($\frac{1}{48}$th) of the Brillouin zone.

III. CALCULATIONS

A. The band structures

Zinc combines with the elements of the VIth column of the Periodic Table, the chalcogenides: O, S, Se, and Te, to form compounds having both the sphalerite and the wurtzite structure, with the single exception of ZnO, which is only found in the latter arrangement. Actually, the ZnO crystal displays a slight distortion of the ideal tetrahedral coordination of the wurtzite structure, with $c/a=1.60$ and $u=0.383$ as compared to the ideal values $c/a=1.63$, $u=0.375$. To study the trends in the electronic properties of the zinc chalcogenides—especially as elucidated by recent Mössbauer experiments with the ^{67}Zn isotope—we have performed LMTO calculations along the lines sketched in Sec. II of the sequence of compounds ZnO, ZnS, ZnSe, and ZnTe, all in the sphalerite structure and at the experimental equilibrium densities, corresponding to cubic lattice constants $a=4.57$, 5.41, 5.67, and 6.07 Å, respectively.[36]

The band structures of ZnS, ZnSe, and ZnTe are shown in Figs. 1–3, while the valence-band densities of states are depicted in Figs. 4–6 including the partial densities of states within each zinc and chalcogen sphere. All calculations used equal radii for all constituent spheres, and the Zn $3d$ electrons were treated as a part of the frozen core, which may be a questionable approximation. In Ref. 37, where the band structure of GaAs was investigated, the relaxation of the $3d$ electrons of Ga was concluded to have some effects on the calculated band energies. Exper-

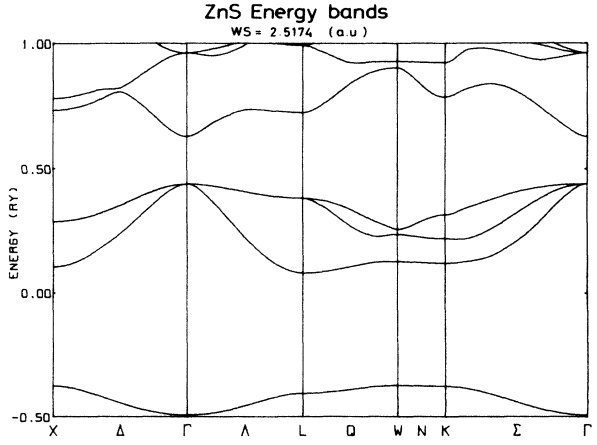

FIG. 1. Band structure of ZnS.

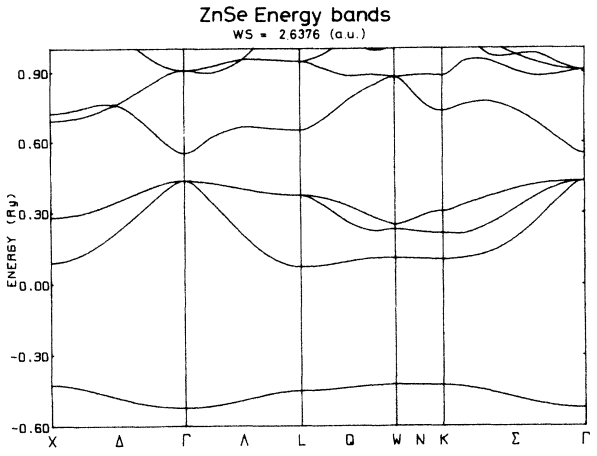

FIG. 2. Band structure of ZnSe.

imentally, the Zn $3d$ electrons of the zinc chalcogenides are known to be located in the gap between the first (anion s-like) and the upper three valence bands.[38] A proper LMTO calculation of the zinc chalcogenides should therefore allow the d electrons to relax and use two panels of energy [i.e., two sets of E_ν's, cf. Eq. (6)], one for the lowest part of the valence bands, the anion s band and the Zn $3d$ bands, and one for the upper three valence bands. Also, spin-orbit coupling ought to be taken into account, as spin-orbit splitting is quite significant, of the order of 0.45 eV in ZnSe and 1 eV in ZnTe.[39–42] In the present work we are mainly interested in the self-consistent charge density, and this we do not expect to be very much dependent neither on spin-orbit coupling nor on the relaxation of $3d$ electrons. Rather, we prefer to keep our calculational scheme at a tractable size.

From Figs. 1–6 the band structures and densities of states of the zinc chalcogenides are seen to be very similar. The lowest band is rather narrow, the width being of the order 1.5 eV, and almost entirely of anion s character. It is separated from the upper three valence bands by a gap of the order of 5 eV. The second band is mixed Zn s-like

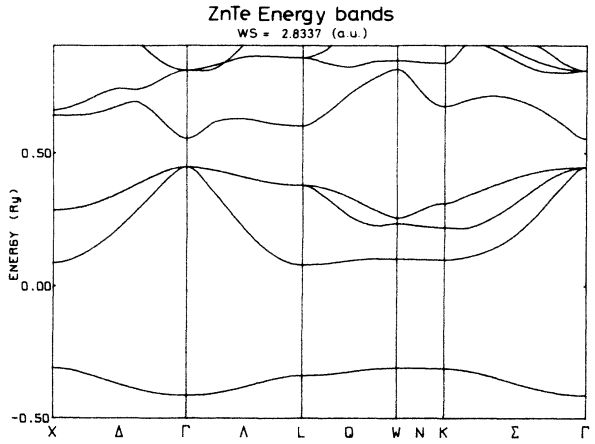

FIG. 3. Band structure of ZnTe.

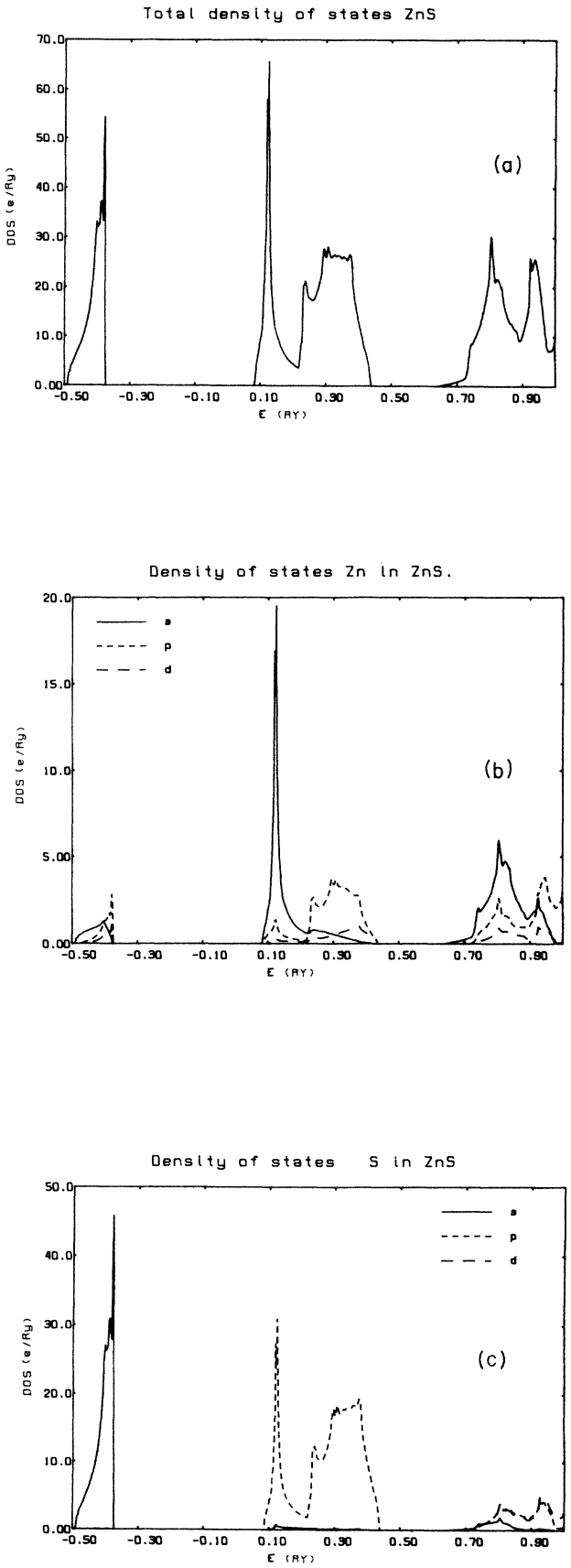

FIG. 4. (a) Total density of states of ZnS. (b) Partial densities of states within the Zn sphere in ZnS. (c) Partial densities of states within the S sphere in ZnS.

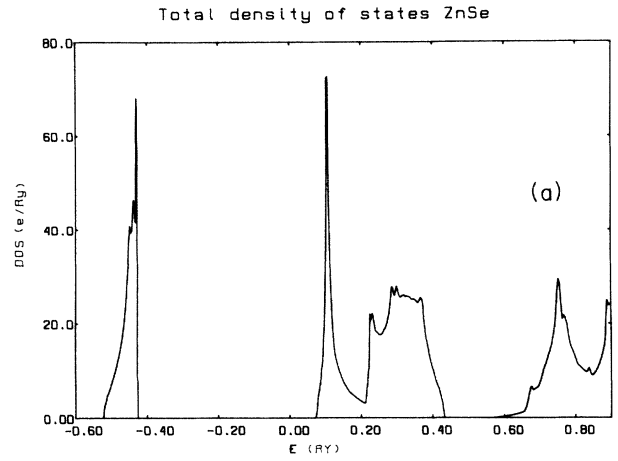

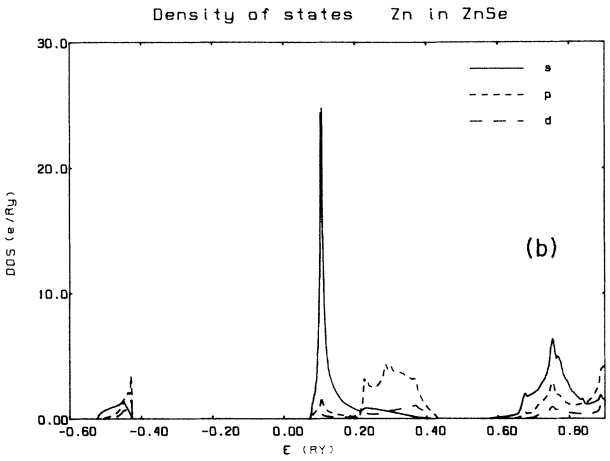

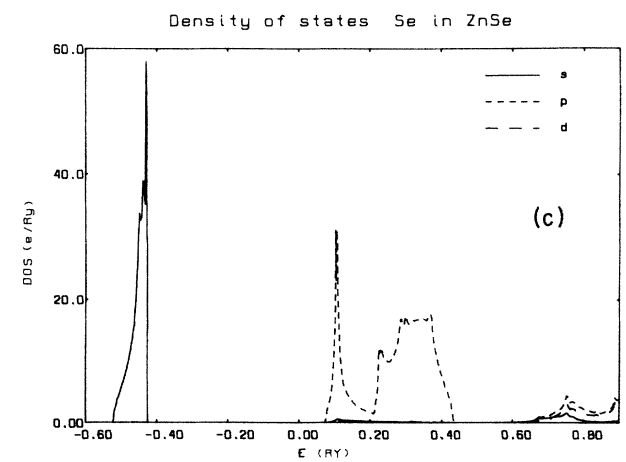

FIG. 5. (a) Total density of states of ZnSe. (b) Partial densities of states within the Zn sphere in ZnSe. (c) Partial densities of states within the Se sphere in ZnSe.

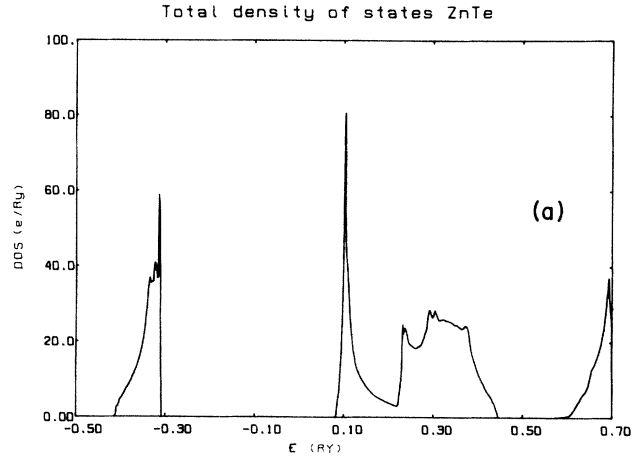

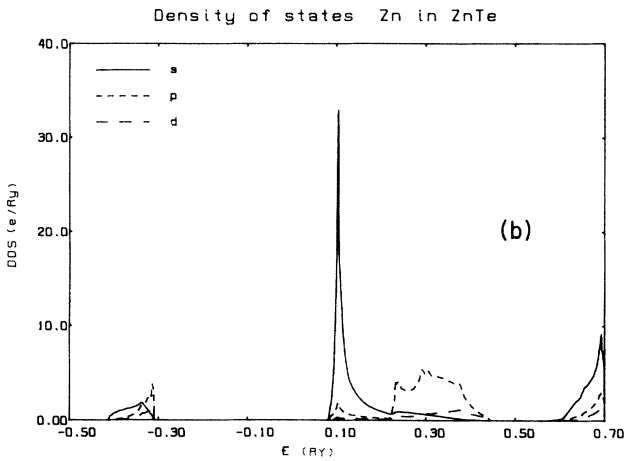

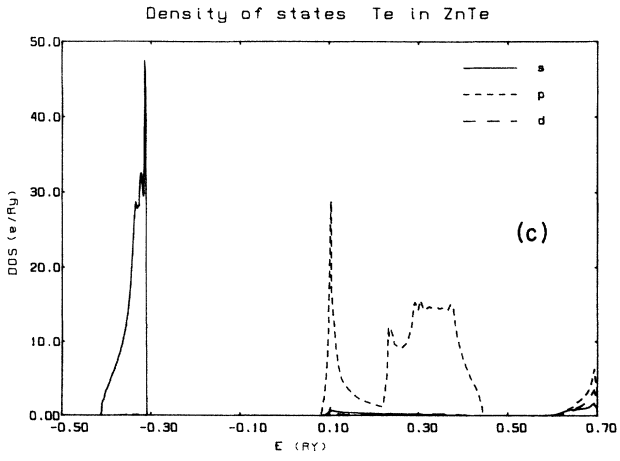

FIG. 6. (a) Total density of states of ZnTe. (b) Partial densities of states within the Zn sphere in ZnTe. (c) Partial densities of states within the Te sphere in ZnTe.

and anion p-like in roughly equal proportion, and the two highest valence bands are entirely anion p-like. The lowest conduction state is the Γ_1 antibonding state, whereby all the calculated zinc chalcogenides become direct-gap semiconductors, in accordance with experiments.

The calculated electron energies at the key symmetry points of the Brillouin zone are listed in Table I, where they are compared to experimental results, which predominantly are from the x-ray photoemission measurements of Ref. 38. The accordance with experimental data is fair but not excellent. Thus, the depth of the anion s band is underestimated by 0.8 eV in ZnS, 2.2 eV in ZnSe, and 1.3 eV in ZnTe. For Ge and GaAs (Ref. 48) discrepancies of $\sim$0 eV and $\sim$0.5 eV for the valence bandwidths are found. Further, the experimental position of the oxygen $2s$ band in (wurtzite) ZnO is 19.5 eV below the valence-band top,[49] to be compared with our calculated (sphalerite) position of $\sim$16.0 eV below the valence-band top. These discrepancies reflect the deficiency of the energy eigenvalues of the local-density approximation to describe properly the removal energies of spatially localized states, a fact which again is traceable to the incomplete elimination of self-interactions within the local-density approximation.[50] From atomic calculations this effect has been estimated to be of the order of 0.8 eV for the As s-like valence band of GaAs,[51] and as large as 8.5 eV for the Ga $3d$ levels of GaAs.[37] However, these numbers probably overestimate the errors of the local-density approximation, as solid-state effects are not taken into account, but they clearly demonstrate the shortcoming of the local-density approximation in this respect.

The widths of the upper three valence bands are also somewhat underestimated by the calculations, by $\sim$1 eV in ZnS and ZnSe and $\sim$0.6 eV in ZnTe. In Ge and GaAs this quantity was found in excellent agreement with experiments.[48] This may be ascribable to the frozen Zn $3d$ electrons and/or—for ZnSe and ZnTe—the neglect of spin-orbit coupling. Thus, the conclusion of Ref. 37 on the relaxation of the Ga $3d$ electrons in GaAs (and inclusion of spin-orbit coupling) was exactly an enlargement of the width of the upper three valence bands. It should, however, also be remembered that the increasing dissimilarity of the constituent atoms in going from the group-IV semiconductors to the III-V to the II-VI semiconducting compounds results in a larger mismatch between the symmetry of the actual electron clouds and the geometry adopted in the calculations through the ASA with spheres of equal size. We are not able to assess the effects hereof, if any.

Focusing next on the conduction bands the zinc chalcogenides are, as mentioned, both experimentally and in the calculations, found to be direct-gap semiconductors, but as is generally found in calculations of semiconductors (see, e.g., Refs. 48 and 42, Table I) within the local-density approximation, the calculated gaps are too small. For ZnS, ZnSe, and ZnTe the calculated gaps are 2.57, 1.60, and 1.45 eV, respectively, as compared to the experimental (0 K) gaps of 3.78, 2.82, and 2.39 eV. For ZnO we

TABLE I. Energy eigenvalues at the Γ, X, and L points, compared to experimental data stemming from Ref. 38, except where noted. Numbers in parentheses denote the experimental uncertainty on the last digit.

	ZnO	ZnS		ZnSe		ZnTe	
	Present	Present	Expt.	Present	Expt.	Present	Expt.
Γ_1	−16.67	−12.68	−13.5(4)	−13.04	−15.2(6)	−11.71	−13.0(4)
Γ_{15}	0.00	0.00		0.00		0.00	
Γ_1	2.26	2.57	3.78[a]	1.60	2.82[a]	1.45	2.39[e]
Γ_{15}	15.44	7.09	7.1[b]	6.43	7.6[c]	4.89	5.1[b]
X_1	−15.24	−11.08	−12.0(3)	−11.72	−12.5(4)	−10.31	−11.6(3)
X_3	−3.69	−4.55	−5.5(2)	−4.69	−5.6(3), −5.3(3)[d]	−4.89	−5.5(2)
X_5	−1.66	−2.03	−2.5(2)	−2.09	−2.1(3)	−2.17	−2.4(2)
X_1	6.48	3.97	4.0(3)	3.52	4.8(3)	2.64	3.7(2)
X_3	10.52	4.62		3.94		2.89	
L_1	−15.56	−11.49	−12.4(3)	−12.05	−13.1(3)	−10.69	−12.0(3)
L_1	−4.45	−4.88	−5.5(2)	−4.93	−5.6(3)	−4.99	−5.5(2)
L_3	−0.58	−0.78	−1.4(4)	−0.83	−1.3(3), −0.7(2)[d]	−0.90	−1.1(3)
L_1	7.14	3.86		2.97		2.10	
L_3	9.25	7.50		6.95		5.53	
$X_1^c - X_5^v$		6.00	6.6,[a] 6.8[b]	5.61	6.42[a]	4.81	5.3[b]
$X_3^c - X_1^c$		0.65	0.5[b]	0.42	0.8[b]	0.25	
$L_1^c - L_3^v$		4.64	5.81,[a] 5.9[b]	3.80	4.9[c]	3.00	3.8[b]
$L_3^c - L_3^v$		8.28	9.8,[a] 9.5[b]	7.78	8.45[c]	6.43	6.6[b]

[a]Reference 43.
[b]Reference 44.
[c]Reference 45.
[d]Reference 46.
[e]Reference 47.

further calculate $E_g = 2.26$ eV to be compared to the (wurtzite) experimental $E_g = 3.44$ eV. Also the secondary gaps at X and L are generally underestimated by the calculations. It has been pointed out[52] that the one-particle potential appropriate for describing the conduction states of semiconductors may deviate from that pertinent to valence states by a constant contribution. The value of this constant is, however, not known. Considerable improvements on the calculated conduction-band edges may be accomplished by a rigid upwards shift, but the fact that the conduction bands cannot be brought in reasonable accordance with experiments by such a procedure demonstrates that other errors of the local-density approximation are significant. Similar results have been found for Si, Ge, and GaAs.[48]

The band structure of (hexagonal) ZnO has been calculated in Ref. 53 using the nonlocal pseudopotential method. Cubic ZnS has been considered theoretically in a number of publications and the electronic band structure has been calculated using the orthogonalized plane-wave (OPW) method,[54–57] the empirical pseudopotential method,[44] tight-binding,[58] APW,[59] Korringa-Kohn-Rostoker (KKR),[60,61] and the linear combination of Gaussian orbitals (LCGO) method.[51] ZnSe has been treated using the pseudopotential method,[44,62,63] OPW,[54,55,45] the LCGO method,[51] and the fully relativistic LMTO method.[41] Finally, ZnTe has been considered using empirical pseudopotentials,[44] OPW,[55,64] and LMTO.[42]

B. The charge distributions

One of the great advantages of the ASA is that it provides a simple and unambiguous angular momentum decomposition of the electron density within the spheres. The integrated number of electrons of s, p, and d character within each sphere thus become convenient numbers characterizing the solids under study. In Table II are listed the occupancy numbers as obtained in the present calculations. Also given are the electron contact densities of the zinc and chalcogen nuclei and the density at the center of each empty sphere. The occupancy numbers are directly related to the way in which the crystal volume is divided into spheres. In comparing the zinc occupancies for the zinc chalcogenides of unequal lattice constants, one may take two different points of view: either to compare occupancy numbers of spheres constituting a fixed fraction of the crystal unit cell or to compare occupancy numbers of spheres of equal absolute volume. The latter approach seems more appealing because of its physical interpretation in terms of atomic sizes within the solid, but as will be demonstrated shortly, the appropriate "size" of the zinc atom actually varies with the ligand in the sequence of zinc compounds studied.

The first approach is facilitated by choosing all spheres of equal size, whereby the zinc spheres cover 25% of space, as was the case for the calculations discussed in Sec. III A. The columns II–IV in Table II refer to these calculations. To be able to take the second approach as well, two additional calculations have been performed for ZnS and ZnTe (columns V and VI of Table II) keeping the Zn sphere volume equal to the one adopted for Zn in ZnSe. To minimize overlap effects, the size of the chalcogen sphere was chosen so as to render the volume covered by the two atomic spheres unchanged. Hereby the ratio of sphere radii approximately equals the ratio of tetrahedral radii introduced by Phillips[65] to describe the bond lengths of tetrahedrally coordinated semiconductors. The radii of the two empty spheres were chosen in the same ratio. For ZnO this approach is not possible, as the oxygen sphere shrinks to almost nothing. In all the calcu-

TABLE II. Calculated data on the electronic structure of the zinc chalcogenides in the sphalerite structure. S is the atomic sphere radius in a.u., $\rho(0)$ the electron contact density in a.u., ρ_{int} the electron density at the center of the empty spheres in 10^{-3} a.u. Q denotes the total charge content of the empty spheres E_1 (surrounding the anions) and E_2 (surrounding the zinc sphere).

		I ZnO	II ZnS	III ZnSe	IV ZnTe	V ZnS	VI ZnTe
$S_{\text{Zn}} = S_{E_1}$		2.125	2.517	2.638	2.834	2.638	2.638
$S_{\text{chal}} = S_{E_2}$		2.125	2.517	2.638	2.834	2.384	3.006
$\rho(0)$	Zn	7.56	8.92	9.28	9.79	8.74	10.00
	chal	14.88	18.66	53.57	107.93	18.66	108.33
ρ_{int}	E_1	3.98	2.52	2.28	2.00	2.55	1.96
	E_2	3.96	2.00	1.71	1.31	1.96	1.36
Zn	n_s	0.33	0.61	0.69	0.83	0.67	0.72
	n_p	0.32	0.64	0.71	0.89	0.76	0.69
	n_d	0.11	0.17	0.18	0.20	0.23	0.13
chal	n_s	1.82	1.68	1.70	1.62	1.60	1.71
	n_p	4.53	3.69	3.44	3.04	3.44	3.66
	n_d	0.01	0.05	0.04	0.05	0.04	0.07
Q	E_1	0.50	0.69	0.73	0.82	0.88	0.57
	E_2	0.37	0.48	0.51	0.55	0.37	0.75

lations quoted in Table II, the atomic cores were kept frozen.

From Table II the valence electron contact density is seen to increase in the sequence of increasing Z of the ligand from ZnO through ZnS and ZnSe to ZnTe, which is also the order of decreasing ionicity according to the Pauling[66] scale of electronegativity. The total relative variation in $\rho(0)$ is $\sim 25\%$, but $\frac{2}{3}$ of this variation is due to the incorporation of ZnO in the calculations. The trend of increasing Zn contact density is accompanied by an increase in the s-electron content of the Zn sphere, both when looking at the fixed-fraction and the fixed-absolute volume series of calculations. This trend must therefore be attributed to the increasing electronegativity of the ligand from Te to O causing electrons of s character to be dragged away from the zinc atom.

The zinc s- and p-occupancy numbers are approximately equal, $n_s \sim n_p$, for all the calculations presented in Table II. The configuration of the zinc atom is therefore far from the atomic ground state $4s^2$ configuration. For the chalcogens one notes an s occupancy close to 2 in accordance with the large binding energy of the free-atom s level, which causes this level to be corelike.

Looking at the occupancy numbers of the calculations I–IV, which dedicate $\frac{1}{4}$ of the unit cell volume to each sphere, a distinct trend is seen when going from ZnO through ZnS and ZnSe to ZnTe, as the total electron content of the zinc sphere increases from 0.76 to 1.92, i.e., for ZnTe the zinc sphere is almost neutral. The chalcogenide sphere charge correspondingly decreases from 6.36 to 4.71, so that the oxygen sphere in ZnO displays an excess of negative charge, while the other compounds all have less than six electrons within the chalcogen sphere. The electron contents of the empty spheres increase in the same sequence. These variations are predominantly due to the different absolute volumes. Thus, one may note that the *mean* electron density within the zinc sphere is much more nearly constant and in fact decreases from ZnS to ZnSe to ZnTe. (The mean density is lowest in ZnO, even though the Zn sphere is smallest in this case. This must therefore reflect that a significant charge transfer to the oxygen atom has taken place.) Likewise, the mean density and central density of the empty spheres actually decreases from ZnO to ZnTe.

The contents of d electrons in the chalcogen spheres are very small. This means that the electron densities within the spheres are almost spherically symmetric, as wave functions of only s and p character lead to spherically symmetric charge densities in cubic symmetry. Thus, we may fear that the electron clouds around the anions actually are larger than the size of the sphere adopted in the calculations. This is also supported by the fact that the electron content of the empty spheres surrounding the anion (the E_1 sphere) is larger than the content of the empty spheres surrounding the Zn sphere (the E_2 sphere), indicating that a tail of the charge density "belonging" to the anion penetrates into the empty sphere. Further, the zinc spheres contain considerably larger amounts of d electrons with correspondingly larger nonspherical charge densities. This may be taken as an indication that the Zn spheres likewise have to account for some of the chalcogen charge.

Considering next the calculations of ZnS, ZnSe, and ZnTe, where the zinc sphere size is kept constant, i.e., columns V, III, and VI of Table II, we note a much smaller variation in the occupancy numbers both for the zinc and the ligand sphere. The zinc occupancies show, as mentioned, an increase of s electrons in going from ZnS to ZnTe, from 0.67 to 0.72, which reflect the decrease of the chalcogen electronegativity in the same sequence. But at the same time the contents of zinc p and d electrons decrease. This implies a larger nonspherical component of the charge distribution around the zinc atom in ZnS than in ZnTe, which seems unreasonable in conjunction with smaller s components. We therefore interpret the numbers as reflecting the spherical charge distribution around the chalcogen penetrating into the zinc sphere, where they show up as nonspherical pockets in the bonding direction, and this being more pronounced in ZnS than in ZnTe. Therefore, at least part of the p and d occupancies of zinc in this series really should be ascribed to the ligand. The effective size of the zinc atom, as deferred from the symmetry of the charge distribution, therefore decreases when combining with lighter (and more electronegative) chalcogen, going from Te to Se to S. This is, in fact, quite sensible, as the increased depletion of charge from the zinc atom allows the charge clouds of the neighbors to come closer to the zinc nucleus.

The chalcogenide occupancies in the same sequence of calculations V, III, VI are remarkably invariant, with about 1.7 s electrons and 3.4 p electrons. The similarity of these numbers is the more surprising, as they both refer to orbitals of different principal quantum number and to different volumes (these have, however, been constructed to more or less mimic the appropriate size of the chalcogen atoms—thus compensating the first point).

We have not undertaken further studies of the consequences of varying the sphere sizes in the zinc chalcogenides, though the above analysis seems to suggest that for each component the best zinc radius could be traced by looking at the variation of the occupancy numbers. However, this comprehensive task is of limited validity for our present purposes. From the electron contact densities in calculations II and V, as well as IV and VI, we get an impression of the variations of this quantity, which the LMTO method renders.

It is tempting at this point to try to estimate the effective charges which should be attributed to the atoms in the zinc chalcogenides. There is, of course, no stringent way of dividing the actual electronic charge distribution in a solid between the constituent atoms, except in the ideal ionic case, where the electron clouds around each nucleus separate, leaving a ball-like picture of the ions in the solid. The net electron transfer in binary compounds therefore remains a qualitative concept depending on the way it is defined but, nevertheless, useful in discussing many properties of solids. Many experiments measure quantities which can be related to an effective charge transfer, though this often depends on the perturbation of the crystal, which the measurement introduces. What is measured is then rather a dynamic charge transfer, which need not be the same as the static charge transfer nor the

same as is measured by other experiments.[67,68]

One reasonable way to arrive at some estimates of the static charge transfer of the zinc chalcogenides is as follows: Assuming that the calculations I, II, III, and VI describe the charge distributions most realistically, we should start from the occupancy numbers for these, and the problem remains how to share the interstitial charges, the contents of E_1 and E_2. For ZnO, ZnS, and ZnSe, where the two empty spheres are equal in size, the charge difference Q_1-Q_2 indicates that the tail of the anion charge distribution sticks out into the E_1 sphere. Assuming that this difference and a similar amount from the cation sphere rightly should be attributed to the anion, while the rest of the interstitial charge may be distributed equally between the two atoms, the following formulas for the effective charges are arrived at:

$$Q_c^*=Q_c+2Q_2-Q_1\ ,$$
$$Q_a^*=Q_a+2Q_1-Q_2\ . \tag{8}$$

Here subscripts c and a refer to cation and anion. For ZnTe, where the sphere sizes are unequal, we propose to split the interstitial charge in the proportion of the anion and cation sphere surface areas.

By this prescription we obtain the effective charge configurations listed in Table III. ZnO is thus attributed a large ionic character, while the other zinc chalcogenides are predicted to be built from predominantly neutral entities, but with the order of decreasing charge transfer to the chalcogen equal to the order of increasing electron contact density, i.e., ZnO, ZnS, ZnSe, ZnTe. The fact that the charge transfer in ZnTe actually goes from Te to Zn according to the above scheme indicates that the prescription suggested is not too reliable. On general grounds we will always expect a group-VI element to be more electronegative than a group-II element. The definition of effective charge given should therefore not be taken too rigorously but just as a way of sorting out the trends in electron transfer.

In Table III are also quoted the effective charges as described from lattice vibrational properties of the zinc chalcogenides.[65] These values vary less amongst each other than the estimates of the present work, but the trend is the same, following the ionicity order. Other calculated properties correlating with this order are likewise given in the table, notably the zinc electron contact density, the fundamental gap, the average gap (defined as the mean of the direct gaps at Γ, X, and L), the bandwidth $\Gamma_{15}^v-\Gamma_1^v$, the width of the upper three valence bands $\Gamma_{15}^v-L_1^v$, the X valence band gap $X_3^v-X_1^v$, and the fractional ionicity as given by the Phillips scale and the Pauling scale.[69] Some anomaly is seen in the band-structure data of ZnS and ZnSe, which we cannot explain, but all other trends are clear. The Phillips spectroscopic scale of ionicity attributes largely the same fraction of ionicity to the bonds of the four compounds considered, thus failing to describe the distinct ionicity of ZnO, which appears in the present work and is, in fact, also predicted by the Pauling ionicity scale.

TABLE III. Various quantities reflecting the ionic character of the zinc chalcogenides.

	ZnO	ZnS	ZnSe	ZnTe
$\rho_{Zn}(0)$[a]	7.5	8.9	9.3	9.8
e^*_{stat}[b]	1.00	0.31	0.13	−0.11
e^*_{lat}[c]	0.53	0.41	0.34	0.27
E_g(direct)[d]	2.26	2.57	1.60	1.45
E_g(average)[d]	6.04	4.40	3.67	3.09
Bandwidth[d]	16.7	12.7	13.0	11.7
$\Gamma_{15}^v-L_1^{vd}$	4.5	4.9	4.9	5.0
$X_3^v-X_1^{vd}$	11.6	6.5	7.0	5.4
$X_{chal}-X_{Zn}$[e]	1.9	0.9	0.8	0.5
f_i(Pauling)[f]	0.80	0.59	0.57	0.53
f_i(Phillips)[f]	0.616	0.623	0.676	0.546

[a]Electron contact density of the zinc nucleus in atomic units.
[b]Estimated static charge transfer as obtained in the present work, in units of e and rendered positive when charge is moved away from Zn.
[c]Effective charge as obtained from lattice vibration spectra, Ref. 65. (The sign of e^* is not given by this method but is chosen positive for all compounds.)
[d]Various characteristics of the band structure, in eV. The average band gap is defined as the mean of the direct gaps at Γ, X, and L.
[e]Difference in Pauling electronegativity.
[f]Fractional ionicity according to the Pauling 1939 and Phillips scales, as quoted by Ref. 69.

IV. CALIBRATION OF THE ^{67}Zn MÖSSBAUER ISOTOPE

The 93.3-keV Mössbauer resonance of ^{67}Zn was first successfully observed by Nagle, Craig, and Keller.[70] This isomer transition is peculiar among all Mössbauer transitions in having the highest relative energy resolution. The natural linewidth of the excited level is $\Gamma_0/E=5\times10^{-16}$. In terms of velocities this corresponds to a broadening of an absorption line of ~0.31 μm/sec. Chemical shifts range over some 200 μm/sec, so considerable sensitivity is obtainable with this isotope, but refined experimental techniques have had to be invented to challenge the extreme theoretical linewidth. The velocity drive generally consists of a piezoelectric element supplied by a sinusoidal voltage.[18,19] For a recent review on ^{67}Zn Mössbauer spectroscopy, see Ref. 11.

The Mössbauer isomer shifts of the zinc chalcogenides ZnO, ZnS, ZnSe, and ZnTe have been measured by two groups.[18,19] Griesinger, Pound, and Vetterling[18] used sources consisting of zinc chalcogenide powders diffused with ^{67}Ga mother nuclei and an enriched ^{67}ZnO absorber. Forster, Potzel, and Kalvius,[19] on the other hand, used a special ^{67}Ga:*Cu* source, which emits a single resonance line, together with enriched absorbers of ^{67}ZnO, ^{67}ZnS, ^{67}ZnSe, and ^{67}ZnTe. Using the samples under study as absorber materials, these authors avoid possible aftereffects of the radioactive decay process of ^{67}Ga. The experimental data of the two groups are in excellent agreement within experimental resolution. However, due to the small velocity shifts of ^{67}Zn, it is important to correct the

measured center shifts for the second-order Doppler shift stemming from the zero-point motion of the ^{67}Zn nuclei.[71] Assuming Debye solids, one may show[71,19] that

$$\Delta V_{\mathrm{SOD}} = 0.23(\mu\mathrm{m/sec})(\Theta_S - \Theta_A) , \tag{9}$$

where Θ_S and Θ_A are, respectively, the source and absorber Debye temperatures, in degrees K. After this correction has been applied, the isomer shifts related to the electronic environment are found. The data of Ref. 19 were corrected in this way, and the isomer shifts obtained are listed in Table IV together with the calculated electron contact densities of the present work, discussed in Sec. III B. The experimental uncertainty stems entirely from the determination of the Debye temperatures to insert in the correction formula (9).

All the contact densities have been calculated for the sphalerite structure at the experimental equilibrium volume, and only the valence electron contribution is quoted, as the frozen core only contributes a constant. As mentioned, ZnO is only found in a slightly distorted wurtzite structure. However, it may be hoped that the difference in electron contact density is not too large between the natural ZnO crystal structure and the hypothetical sphalerite ZnO. Supporting evidence is rendered from ZnS, which exists in both structures, and where no difference in isomer shift is experimentally resolvable.[18,19] Yet, due to the larger ionic character of the ZnO bond, the difference between the contact densities of the two structures may be more profound in ZnO.

Table IV lists the electron contact densities as obtained in the sequence of calculations using equally large spheres for all constituents as well as those obtained for ZnS and ZnTe using different sphere sizes. From these values we obtain an average contact density $\rho_{\mathrm{av}}(0)$, as given in the last column of Table IV, together with a calculational uncertainty of ~ 0.1 a.u. For ZnO we (due to the different crystal structure, but somewhat arbitrarily) set the uncertainty on the calculated $\rho(0)$ higher. The experimental isomer shifts are plotted against the electron contact density in Fig. 7. The linearity is quite good, confirming Eq. (1). From the best straight line, using (2) and (3) and Ref. 13, we obtain

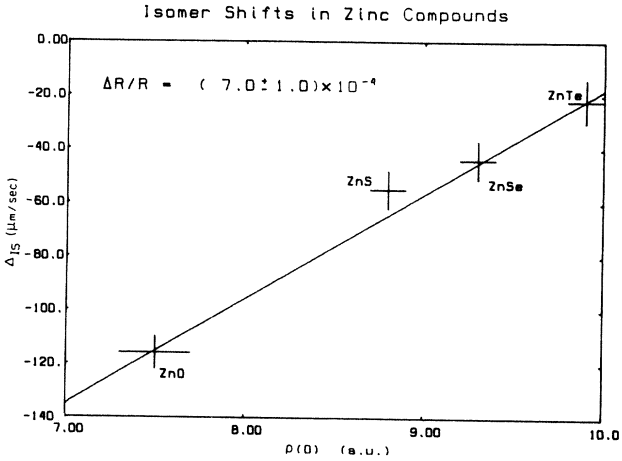

FIG. 7. Experimental isomer shifts versus calculated electron contact densities in the Zn chalcogenides.

$$\frac{\Delta R}{R} = (7.0 \pm 1.0) \times 10^{-4} \tag{10}$$

for the nuclear calibration constant.

The only value of this parameter which has been reported is in Ref. 19, which used the concept of isoelectronic pairs of compounds to obtain $\Delta\langle r^2\rangle = 11 \times 10^{-3}$ fm^2. Converting by (3) and Ref. 13, this corresponds to $\Delta R/R = 3.8 \times 10^{-4}$. The authors stress, however, that this can only be regarded as an order of magnitude estimate, due to the crude character of the argument. The accordance with the value (10) of the present work may therefore be taken to be satisfactory.

Finally, to address the question of the validity of the frozen-core approximation in calculations of the electron contact density, we report in Table V the results of self-consistent fully relativistic atomic calculations (LDA, in the parametrization of von Barth and Hedin[72]) of Zn in various valence configurations. The contact density is split up into the core contribution (i.e., from [Ar]$3d^{10}$) and the valence contribution. Looking at $\rho_{\mathrm{val}}(0)$ of this table, we conclude that the situation in the tetrahedral zinc chalcogenides corresponds to an atomic number of s electrons around or somewhat less than one. Leaving the

TABLE IV. Experimental isomer shifts, Ref. 19, and calculated electron contact densities. The experimental values are all relative to the ^{67}Ga:*Cu* source. The electron contact density is in a.u., ρ_1 corresponds to the fixed fraction series of calculations, I-IV of Table II, ρ_2 to the fixed-absolute-volume series V-III-VI. Numbers in parentheses denote the uncertainty on the last digit.

	Δ_{IS} (μm/sec)	$\rho_1(0)$	$\rho_2(0)$	$\rho(0)$
ZnTe	−22(8)	9.79	10.00	9.9(1)
ZnSe	−44(7)	9.28	9.28	9.3(1)
ZnS(wu)	−55(7)			
ZnS(sph)	−55(7)	8.92	8.74	8.8(1)
ZnO(wu)	−116(6)			7.5(2)
ZnO(sph)		7.56		

TABLE V. Electron contact densities as calculated in several atomic configurations of Zn. $\rho_{\mathrm{core}}(0)$ is the contribution from the [Ar]$3d^{10}$ core, $\rho_{\mathrm{val}}(0)$ the contribution from the fourth shell. (All values are in a.u.)

Valence configuration	$\rho_{\mathrm{core}}(0)$	$\rho_{\mathrm{val}}(0)$
$4s^2 4p^0$	24 607.82	16.69
$4s^1 4p^1$	24 607.75	9.81
$4s^1 4p^0$	24 607.97	10.12
$4s^0 4p^2$	24 607.75	0.06
$4s^0 4p^1$	24 607.87	0.05
$4s^0 4p^0$	24 608.55	0.00

Zn^{2+} ion out, the core contribution varies by only 0.22 a.u. The variation of the self-consistently relaxed Zn core in the sequence ZnO, ZnS, ZnSe, ZnTe is expected to be some fraction of this (but presumably systematic)—that is, of negligible importance in comparison with the general accuracy of the LMTO method discussed above. As a matter of fact, we only find reasons for worrying about the frozen-core approximation when the Zn atom approaches full ionization, i.e., $4s^0 4p^0$, but even in the case of highest ionicity treated here, ZnO, is the effective electronic configuration of Zn far from this extreme.

Further information to gain from Table V is the size of the contribution from the relativistic $p_{1/2}$ electrons to the valence electron contact density, which is neglected throughout our solid-state calculations. It is of the order of 0.05 a.u., again barely of significance at the present level of accuracy. Similar conclusions have been drawn for Sn in various atomic configurations,[73,74] as well as for other atoms.[75]

V. CONCLUSIONS

The electronic structure of the zinc chalcogenides was calculated from first principles and compared to recent Mössbauer experiments using the extremely narrow resonance of the ^{67}Zn isotope. A good accordance was found providing for the first time a quantitatively reliable calibration constant for this isotope. This should facilitate a more extensive use of ^{67}Zn spectroscopy for the study of solid-state systems in the future.

The electronic band structures of the zinc chalcogenides were as good as those obtained from any other first-principles method, but the agreement with experiments is only qualitatively correct, while quantitative band-edge positions and transition energies are not correct. This is presumed to be a deficiency of the LDA.

The LMTO method is ideal for the purpose of calibrating Mössbauer isotopes for several reasons. Firstly, this scheme uses the real (as opposed to pseudo) potential of the core, so that the derived ground-state charge density is correct, even in the nuclear region. The electron contact density is then simply read off as the charge density in the center of the atomic sphere (or more appropriate, by averaging the charge density over the nuclear volume). Secondly, for the interpretation of isomer shifts, the decomposition of the LMTO wave function into orbital angular momentum channels provides the occupancy numbers, which conveniently are used to characterize the solids under study, as demonstrated in the present work for the zinc chalcogenides. Thirdly, the LMTO scheme is easy to handle and fast, and, if necessary, one can relatively easily switch to another crystal structure, as long as this is not too complicated. Thus, the calculation of several different crystal structures for the calibration of the same isotope is possible, as has been utilized by the present authors in the cases of ^{119}Sn, ^{121}Sb, ^{125}Te, and ^{73}Ge.[74]

ACKNOWLEDGMENT

The authors would like to express their gratitude to Dr. H. L. Skriver, who supplied them with a full copy of his LMTO codes.

*Present address: Max-Planck-Institut für Festkörperforschung, Heisenbergstrasse, 1, D-7000 Stuttgart 80, Federal Republic of Germany.

[1] *Mössbauer Isomer Shifts,* edited by G. K. Shenoy and F. E. Wagner (North-Holland, Amsterdam, 1978).

[2] G. Weyer, A. Nylandsted-Larsen, B. I. Deutch, J. U. Andersen, and E. Antoncik, Hyperfine Interact. **1**, 93 (1975).

[3] J. De Bruyn, R. Coussement, I. Dezsi, G. Langouche, and M. Van Rossum, Hyperfine Interact. **10**, 973 (1981).

[4] G. Weyer, J. W. Petersen, S. Damgaard, H. L. Nielsen, and J. Heinemeier, Phys. Rev. Lett. **44**, 155 (1980); G. Weyer, J. W. Petersen, and S. Damgaard, in *Proceedings of the 12th International Conference on Defects in Semiconductors,* edited by C. A. J. Ammerlaan (North-Holland, Amsterdam, 1982), p. 470.

[5] E. Antoncik, Hyperfine Interact. **11**, 265 (1981).

[6] E. Antoncik and B. L. Gu, in *Proceedings of the 12th International Conference on Defects in Semiconductors,* edited by C. A. J. Ammerlaan (North-Holland, Amsterdam, 1982), p. 127.

[7] E. Antoncik and B. L. Gu, Hyperfine Interact. **14**, 257 (1983).

[8] O. H. Nielsen, F. K. Larsen, S. Damgaard, J. W. Petersen, and G. Weyer, Z. Phys. B **52**, 99 (1983).

[9] D. W. Hafemeister and H. de Waard, Phys. Rev. B **7**, 3014 (1973).

[10] G. Weyer, H. Andreasen, and H. de Waard, Phys. Status Solidi B **132**, 219 (1985).

[11] T. Katila and K. Riski, Hyperfine Interact. **13**, 119 (1983).

[12] B. D. Dunlap and G. M. Kalvius, Ref. 1, Chap. 2.

[13] G. K. Shenoy and B. D. Dunlap, Ref. 1, Appendix IV.

[14] R. A. Uher and R. A. Sorensen, Nucl. Phys. **86**, 1 (1966). See also, J. Speth, W. Henning, P. Kienle, and J. Meyer, Ref. 1, Chap. 13.

[15] E. Antoncik, Phys. Rev. B **23**, 6524 (1981).

[16] T. C. Tucker, L. D. Roberts, C. W. Nestor, T. A. Carlsson, and F. B. Malik, Phys. Rev. **178**, 998 (1969).

[17] E. Antoncik and B. L. Gu, Phys. Status Solidi B **111**, 261 (1982).

[18] D. Griesinger, R. V. Pound, and W. Vetterling, Phys. Rev. B **15**, 3291 (1977).

[19] G. M. Forster, W. Potzel, and G. M. Kalvius, Z. Phys. B **37**, 209 (1980).

[20] O. K. Andersen, Phys. Rev. B **12**, 3060 (1975).

[21] H. L. Skriver, *The LMTO Method* (Springer, Berlin, 1984).

[22] P. Hohenberg and W. Kohn, Phys. Rev. **136**, B864 (1964); W. Kohn and L. J. Sham, Phys. Rev. **140**, A1133 (1965).

[23] *Theory of the Inhomogeneous Electron Gas,* edited by S. Lundqvist and N. H. March (Plenum, New York, 1983).

[24] D. M. Ceperley, Phys. Rev. B **18**, 3126 (1978); D. M. Ceperley and B. J. Alder, Phys. Rev. Lett. **45**, 566 (1980).

[25] S. H. Vosko, L. Wilk, and M. Nusair, Can. J. Phys. **58**, 1200 (1980).

[26] J. Keller, J. Phys. C **4**, L85 (1971).

[27] H. L. Skriver, Phys. Rev. B **31**, 1909 (1985).

[28] M. T. Yin and M. L. Cohen, Phys. Rev. B **26**, 5668 (1982); R. Biswas, R. M. Martin, R. J. Needs, and O. H. Nielsen, *ibid.* **30**, 3210 (1984).

[29] Electronic Structure, Dynamics and Quantum Structural Properties of Condensed Matter, edited by J. T. Devreese, V.

E. Van Doren, and P. E. Van Camp (Nato Advanced Study Institute, Antwerp, 1984).
[30]D. Glötzel, B. Segall, and O. K. Andersen, Solid State Commun. **36**, 403 (1980).
[31]T. Jarlborg and A. J. Freeman, Phys. Lett. **74A**, 349 (1979).
[32]N. E. Christensen, Phys. Rev. B **30**, 5327 (1984).
[33]Actually, in this work the radial Dirac equation is used, with the spin-orbit term omitted (the scalar relativistic approximation) as described in Ref. 21, p. 219.
[34]The correction for the nonspherical potential variation consists of the addition of the extra terms $\langle \chi_{L'} | \Delta V | \chi_L \rangle$ to the Hamiltonian, where ΔV is the leading ($l=3$) nonspherical potential component. The evaluation of these matrix elements is performed over atomic spheres, thus neglecting overlaps and also ignoring the fact that the combined correction term very crudely corrects for nonsphericity in the overlap regions.
[35]O. Jepsen and O. K. Andersen, Solid State Commun. **9**, 1763 (1971); G. Lehman and M. Taut, Phys. Status Solidi B **54**, 469 (1972).
[36]R. W. G. Wyckoff, *Crystal Structures I,* 2nd ed. (Wiley, New York, 1965).
[37]G. B. Bachelet and N. E. Christensen, Phys. Rev. B **31**, 879 (1985).
[38]L. Ley, R. A. Pollak, F. R. McFeely, S. P. Kowalczyk, and D. A. Shirley, Phys. Rev. B **9**, 600 (1974).
[39]*Landolt-Börnstein: Zahlenwerte und Funktionen aus Naturwissenscaften und Technik* (Springer-Verlag, New York, 1982), Vol. III, p. 176.
[40]Very recent LMTO calculations on ZnSe (Ref. 41) and ZnTe (Ref. 42) have used this more accurate approach for the purpose of studying deformation potentials and pressure-dependent structural properties and phase transformations. For these latter applications, where the total energy needs to be calculated, it is essential to allow for the 3*d* electrons to relax, whereas spin-orbit coupling seems to have only minor effects. The fact that the fundamental gaps of the present calculations are somewhat larger than those of Refs. 41 and 42 is probably due to the inclusion of the leading nonspherical component of the potential within the spheres, or a combined effect of this and the frozen Zn 3*d* electrons.
[41]S. Ves, K. Strössner, N. E. Christensen, Chul Koo Kim, and M. Cardona, Solid State Commun. (to be published).
[42]N. E. Christensen and O. B. Christensen (unpublished).
[43]D. Theis, Phys. Status Solidi B **79**, 125 (1977).
[44]M. L. Cohen and T. K. Bergstresser, Phys. Rev. **141**, B789 (1966).
[45]P. M. Raccah, R. N. Euwema, P. J. Stukel, and T. C. Collins, Phys. Rev. B **1**, 756 (1970).
[46]W. D. Grobman, D. E. Eastman, and J. L. Freeouf, Phys. Rev. B **12**, 4405 (1975).
[47]R. E. Nahary and H. Y. Fan, Phys. Rev. Lett. **17**, 251 (1966).
[48]A. Svane (unpublished). See also Ref. 37.
[49]W. Ranke, Solid State Commun. **19**, 685 (1976).
[50]A. R. Williams and U. von Barth, Ref. 23, Chap. 4.
[51]C. S. Wang and B. M. Klein, Phys. Rev. B **24**, 3393 (1981).
[52]J. P. Perdew and M. Levy, Phys. Rev. Lett. **51**, 1884 (1983); L. J. Sham and M. Schlüter, *ibid.* **51**, 1888 (1983).
[53]J. R. Chelikowsky, Solid State Commun. **22**, 351 (1977).
[54]D. J. Stukel, R. N. Euwena, T. C. Collins, F. Herman, and R. L. Kortum, Phys. Rev. **179**, 740 (1969).
[55]G. G. Wepfer, T. C. Collins, and R. W. Euwema, Phys. Rev. B **4**, 1296 (1971).
[56]F. Herman, R. L. Kortum, C. Kuglin, and I. Shay, *Proceedings of the International Conference on II-VI Semiconducting Compounds,* edited by D. G. Thomas (Benjamin, New York, 1967).
[57]O. V. Forberovich, S. I. Kurganskii, and E. P. Doma-Shevskaya, Phys. Status Solidi B **97**, 63 (1980).
[58]S. T. Pantelides and N. A. Herrison, Phys. Rev. B **11**, 3006 (1975).
[59]U. Rössler and M. Lietz, Phys. Status Solidi **17**, 597 (1966).
[60]P. Eckelt, O. Madelung, and J. Trensch, Phys. Rev. Lett. **18**, 656 (1967).
[61]P. Eckelt, Phys. Status Solidi **23**, 307 (1967).
[62]J. R. Chelikowsky and M. L. Cohen, Phys. Rev. B **14**, 556 (1976).
[63]T. P. Humphreys and G. P. Srivastava, Phys. Status Solidi B **112**, 581 (1982).
[64]F. Herman, R. L. Kortum, C. D. Kuglin, J. P. Van Dyke, and S. Skillman, in *Methods of Computational Physics,* edited by B. J. Alder, S. Fenbach, and M. Rotenberg (Academic, New York, 1968), Vol. 8.
[65]J. C. Phillips, *Bonds and Bands in Semiconductors* (Academic, New York, 1973).
[66]L. Pauling, *The Nature of the Chemical Bond,* 3rd ed. (Cornell University Press, New York, 1960).
[67]C. Hilsum and A. C. Rose-Innes, *Semiconducting III-V Compounds* (Pergamon, New York, 1961).
[68]E. Antoncik, in *Proceedings of the 17th International Conference on the Physics of Semiconductors,* edited by J. D. Chadi and W. A. Harrison (Springer, New York, 1985), p. 1017.
[69]J. C. Phillips, Rev. Mod. Phys. **42**, 317 (1970).
[70]D. E. Nagle, P. P. Craig, and W. E. Keller, Nature **186**, 707 (1960); P. P. Kraig, D. E. Nagle, and D. R. F. Cochran, Phys. Rev. Lett. **4**, 397 (1960).
[71]G. K. Shenoy, F. E. Wagner, and G. M. Kalvius, Ref. 1, Chap. 3.
[72]U. von Barth and L. Hedin, J. Phys. C **5**, 1629 (1972).
[73]S. L. Ruby and G. K. Shenoy, Ref. 1, Chap. 9b.
[74]A. Svane and E. Antoncik (unpublished).
[75]A. J. Freeman and D. E. Ellis, Ref. 1, Chap. 4.